7th Trondheim CCS Conference, TCCS-7, June 5–6 2013

# Frictional pressure drop for two-phase flow of carbon dioxide in a tube: Comparison between models and experimental data

Frøydis Aakenes[a], Svend Tollak Munkejord[b,*], Michael Drescher[b,c]

[a]*Norwegian University of Science and Technology, Dept. of Energy and Process Engineering, NO-7491 Trondheim, Norway*
[b]*SINTEF Energy Research, P.O. Box 4761 Sluppen, NO-7465 Trondheim, Norway*
[c]*Statoil ASA, Arkitekt Ebbells veg 10, NO-7005 Trondheim, Norway*

## Abstract

We compare models for two-phase frictional pressure drop with experimental data for pure $CO_2$ taken in a tube of 10 mm inner diameter. The flow was nearly adiabatic, and the mass fluxes ranged from 1058 to 1663 kg/(m$^2$ s), the saturation temperatures were between 3.8 and 17 °C, and the vapor fractions varied from 0.099 to 0.742. Three models for frictional pressure drop were considered, namely a simple model assuming homogeneous flow, the model of Friedel, and the model of Cheng *et al.* The Friedel model is a curve fit to experimental data based on dimensionless groups, while the Cheng *et al.* model includes phenomenological sub-models. Our data indicate that the Friedel model is preferable for $CO_2$-transport purposes, at least for high mass fluxes. However, for flowing vapour fractions above 0.6, the Cheng *et al.* model also gives good results. A reason why the Friedel model performs better when compared to our data, may be the fact that it is based on a large experimental database. Further, our mass fluxes are higher than the ones employed by Cheng *et al.*

*Keywords:* $CO_2$ transport, carbon dioxide, frictional pressure drop, correlation, model

## 1. Introduction

According to the Intergovernmental Panel on Climate Change (IPCC), $CO_2$ is the most important anthropogenic greenhouse gas. This is the motivation for the $CO_2$ Capture and Storage (CCS) technology, in which $CO_2$ is 1) captured at the power plants or from other industrial applications, 2) transported, and then 3) injected and stored in geological formations. Thus, problems related to the use of fossil fuel are reduced.

Injection of $CO_2$ into reservoirs for enhanced oil recovery (EOR) has been done since the 1970s. Further, there are by now eight commercial-scale CCS projects in operation around the globe for EOR (Val Verde Natural Gas Plants (USA), Enid Fertilizer (USA), Shute Creek Gas Processing Facility (USA), Great Plains Synfuels Plant and Weyburn-Midale Project (Canada), and Century Plant (USA)) and for storage in saline aquifers (Sleipner $CO_2$ Injection (Norway), In Salah $CO_2$ Storage (Algeria)[1] and Snøhvit $CO_2$ Injection

---

*Corresponding author. Tel: +47 73593897; fax: +47 73592889.
*Email address:* svend.t.munkejord@sintef.no (Svend Tollak Munkejord)
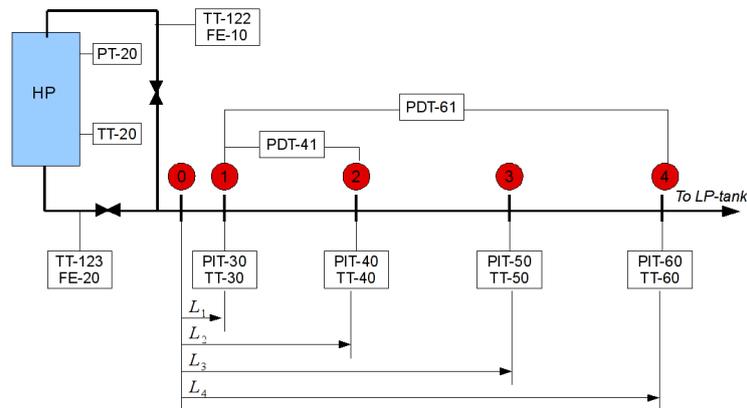[1]$CO_2$ injection is currently suspended at In Salah [1].

Figure 1: The test rig. Sensors measuring absolute pressure (PIT and PT), differential pressure (PDT), temperature (TT) and mass flow rates (FE) are placed as shown. $L_1 = 0.2$ m, $L_2 = 50.5$ m, $L_3 = 101$ m and $L_4 = 139$ m.

(Norway)) and the capacity for storage is considered to be large and safe [2]. Thus, the technology of CCS is regarded as promising [3]. However, there are still several challenges in all the three fields – capture, transportation and storage. Here we consider $CO_2$ transportation.

In $CO_2$ transport by pipeline, the $CO_2$ will often be in a single-phase dense or supercritical state. Nevertheless, two-phase flow can occur in several situations, such as during start-up, pressure release, due to intermittent supply of $CO_2$, or during normal operation [4]. To calculate the flow in such situations, transient simulators need models for the frictional pressure drop, among other things. A good estimate of the pressure drop is needed in order to design the pumps (or compressors) of the pipeline system. Further, for two-phase flow of $CO_2$, the fluid temperature is a function of the pressure. An overview of the state of the art regarding transient simulation of $CO_2$ mixtures in pipelines was given by Aursand *et al.* [5].

Most of the existing flow maps and pressure-drop data for $CO_2$ were taken for heat exchanger applications with tubes with a hydraulic diameter in the millimeter range [6, 7, 8, 9]. In this work, based on the report of Aakenes [10], we compare models for frictional pressure drop with experimental data for pure $CO_2$ taken in a tube of 10 mm inner diameter [11]. See also de Koeijer *et al.* [12]. Three models for frictional pressure drop were considered, namely a simple model assuming homogeneous flow, the model of Friedel [13], and the model of Cheng *et al.* [9]. The Friedel model is a curve fit to experimental data based on dimensionless groups, while the Cheng *et al.* model includes phenomenological sub-models.

The rest of this paper is organized as follows. In Section 2, the experimental set-up is described. The employed frictional pressure-drop models are briefly presented in Section 3, while Section 4 compares experimental data with model predictions and discusses the results. Section 5 concludes the paper.

## 2. Experimental set-up

At Statoil Research Center Rotvoll in Trondheim, a $CO_2$ pipeline test rig is built with the purpose of understanding the physics related to transportation of $CO_2$ [12, 14]. The results used in this work are obtained from six steady-state two-phase pressure-drop experiments [11].

### 2.1. Experimental facility

The test rig consists of a 139 m long pipe with an inner diameter of 10 mm, where the inlet is connected to a high-pressure (HP) tank and the outlet is connected to a low-pressure tank, see Figure 1. The pressure, temperature and mass flow rates are measured by several sensors as shown in the figure. For continuous operation, a compressor and a pump are used for transporting the $CO_2$ back from the low-pressure tank into the high-pressure tank.

Table 1: Overview of the experimental conditions in [11].

| Variable | Range |
| --- | --- |
| Mass flux, $G = \dot{m}/A$ (kg/(m$^2$ s)) | 1058–1663 |
| Flowing vapor fraction, $x = \dot{m}_{\text{g}}/\dot{m}_{\text{tot}}$ (–) | 0.099–0.742 |
| Saturation temperature, $T$ (°C) | 3.8–17 |
| Reduced pressure, $p_r$ (–) | 0.52–0.72 |
| Heat flux, $q''$ (W/m$^2$) | −91–150.8 |

Table 2: Sensor uncertainties.

| Source | Uncertainty |
| --- | --- |
| Temperature sensor, $T$ | ±0.5 K |
| Absolute-pressure sensor, $p$ | ±0.16 bar |
| Differential-pressure sensor, $\Delta p$ | ±0.05 bar |
| Gas-flow meter, $\dot{m}_G$ | ±0.06 % |
| Liquid-flow meter, $\dot{m}_L$ | ±0.3 % |

## 2.2. The experiments

Six experiments have been carried out in the test rig. The experiments were run until steady state was obtained, then the pressure, temperature and mass flow rate were logged over a period of about 20 minutes. In further calculations, the average of the measurements at each location have been used. An overview of the conditions in the experiments are given in Table 1. The experimental data can be found in Appendix A.

The following assumptions have been made in the data analysis. The position numbers in the following are referring to Figure 1.

- The fluid is in a saturated state throughout the pipe test section (from position 1–4).

- The enthalpy is constant through the throttling valves.

- The frictional pressure drop between the HP tank and position 1 is neglected (except from the friction due to the throttling valves).

- Any heat loss between HP tank and position 1 is neglected.

- Any mixing losses at the point where the gas stream and liquid stream meet are neglected.

Further details are given in the report of Aakenes [10, Ch. 7].

An uncertainty analysis has been carried out [10, Ch. 8]. The estimated total uncertainty in the sensors (about 2.5 standard deviations) are listed in Table 2.

The friction-model predictions are sensitive to the uncertainties in the measured quantities. This sensitivity has been estimated for one representative data point. All the models are the most sensitive to the flowing vapor fraction, $x$, and to the mass flux, $G$. The total sensitivity ranged from ±0.024 bar between positions 1 and 2 to ±0.121 bar between positions 1 and 4.

## 3. Frictional pressure-drop models

In a control-volume analysis of single-phase flow in a pipe, the wall-friction force will appear as an external force acting on the fluid control volume. It is typically modeled as

$$F_{\text{w}} = \frac{1}{2} \frac{f|G|G}{\rho d_{\text{h}}} \tag{1}$$

where the friction factor $f = f(Re, \varepsilon_{\text{r}})$ is a function of the Reynolds number, $Re$, and the relative pipe roughness, $\varepsilon_{\text{r}}$. $\rho$ is the density, $G$ is the mass flux and $d_{\text{h}}$ is the hydraulic diameter of the pipe.

In the *Friedel model* [13], the wall-friction force is calculated as

$$F_{\mathrm{w}} = \frac{1}{2} \frac{f_{\ell o} |G| G}{\rho_\ell d_{\mathrm{h}}} \Phi, \tag{2}$$

where $f_{ko} = f(Re_{ko}, \varepsilon_{\mathrm{r}})$ is the friction factor calculated as if the whole flow were phase $k$, and

$$Re_{ko} = \frac{|G| d_{\mathrm{h}}}{\mu_k}. \tag{3}$$

$\Phi$ is a two-phase frictional multiplicator

$$\Phi = \Phi(Fr, We, f_{go}, f_{\ell o}, \rho_{\mathrm{h}}, \rho_{\mathrm{g}}, \rho_\ell, \mu_{\mathrm{g}}, \mu_\ell, x). \tag{4}$$

This is an empirical correlation based on the Froude number, *Fr*, Weber number, *We*, the gas-only and liquid-only friction factors, the two-phase homogeneous flow mixture density, gas and liquid densities, the gas and liquid viscosities, and the flowing vapor fraction (i.e. the vapor fraction based on the mass flow). Due to space limitations, we refer to [13, 10] for details.

The *Cheng et al. model* [9] is not only an empirical fit, but it also employs phenomenological modeling of the flow patterns occurring in the pipe. Details can be found in [9, 10].

The *homogeneous model* is probably the simplest model for two-phase flow. Herein, the density, viscosity and mean velocity are calculated for the two-phase flow assuming no slip between the phases. Details can be found in [10] or e.g. in [15, Sec. 2.3.2].

## 4. Results and discussion

### 4.1. Calculations

The modeled pressure-drop between location 1 and $N$ (see Figure 1) is calculated the following way:

$$\Delta p_{1-N} = \sum_{i=1}^{N} \frac{1}{2} \left( \left. \frac{\partial p}{\partial x} \right|_i + \left. \frac{\partial p}{\partial x} \right|_{i+1} \right) \Delta x_i, \tag{5}$$

where $\Delta x_i$ is the distance between location $i$ and $i + 1$, and $\partial p / \partial x|_i$ is the pressure gradient given by the friction model at location $i$. The calculations are based on saturated fluid properties predicted by NIST [16] at the pressure given by the absolute-pressure sensors at each location.

The calculated $\Delta p_{1-2}$ and $\Delta p_{1-4}$ for each experiment are compared to the experimental pressure drop measured by PDT-41 and PDT-61, respectively (see Figure 1).

Note that the heat flux, $q''$, is set to 0 when using the Cheng *et al.* model. This is because the model does not handle the negative heat flux occuring in some of the experiments. Since the heat flux is relatively small, the error due to this assumption will be negligible.

An illustration of the flow patterns predicted by the Cheng *et al.* model for the four locations in each experiment is shown in Figure 2. The flow-pattern maps are not exactly the same for every experiment and each location, this is the reason for thick transition lines.

### 4.2. Results

The experimental pressure drop and the pressure drop predicted by the friction model between position 1–2, and 1–4, are plotted in Figure 3. The 45-degree line indicates where the friction model predicts the pressure drop exactly, and the two neighboring dashed lines represent the calculated relative standard-deviation (see the equation 6 and Table 3 in the following). This value can be interpreted as the uncertainty in the friction model itself. The uncertainty in the differential-pressure sensors is represented as a horizontal bar accompanied by each dot. The friction-model-input sensitivity is represented as a vertical bar accompanying each dot. As seen, the friction-model-input uncertainty and the sensor uncertainty are small compared to uncertainty in the friction model itself. Thus, the experimental uncertainty is not considered as important when deciding what friction model is the most accurate.
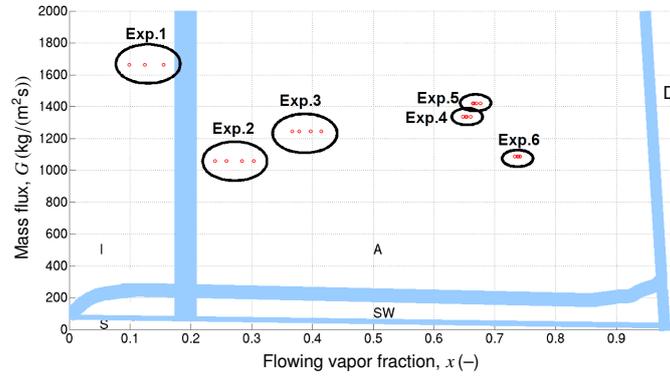
Figure 2: Flow patterns predicted by the Cheng *et al.* model for each experiment. S: Stratified, SW: Stratified-wavy, I: Intermittent, A: Annular, D: Dry-out.

Table 3: Friction-model error calculated based on all the present experiments.

| Model | $s_R$ (%) | $\bar{e}$ (%) |
|---|---|---|
| Friedel | 9.7 | 8.13 |
| Cheng *et al.* | 57.74 | 19.93 |
| Homogenous | 29.18 | 19.11 |

### 4.2.1. Model-error estimation

The models' ability to predict the pressure drop can be represented by the *relative standard deviation* or the *mean error*.

The relative standard deviation is used by Friedel [13] and is calculated as

$$s_R = \Big(\frac{1}{N-1} \sum_i z_i^2\Big)^{1/2},\tag{6}$$

where

$$z_i = \frac{\Delta p_{i,\text{exp}} - \Delta p_{i,\text{pred}}}{\Delta p_{i,\text{pred}}}.\tag{7}$$

Herein, the subscript "exp" refers to the experimental value and "pred" is the predicted value.
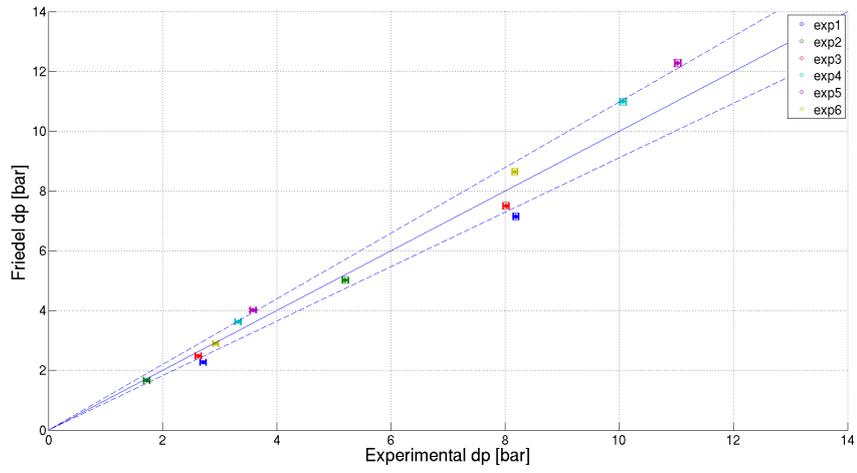
An alternative way to represent the accuracy of the friction models is by the *mean error*. It is used by Cheng *et al.* [9] and is defined as

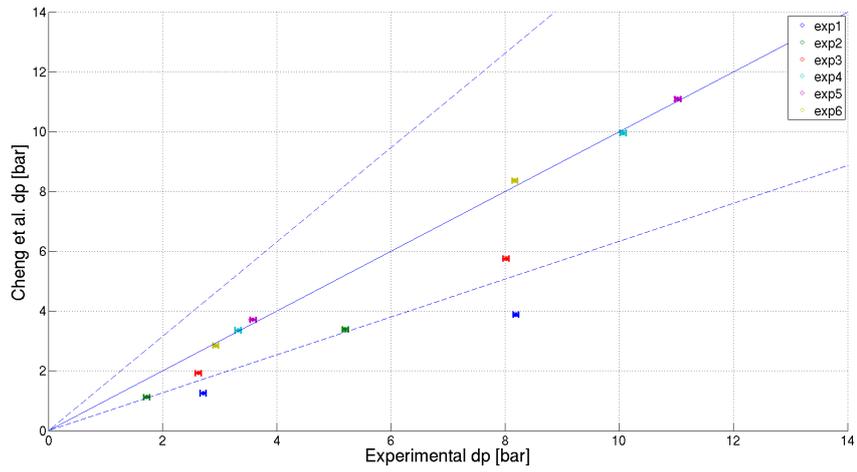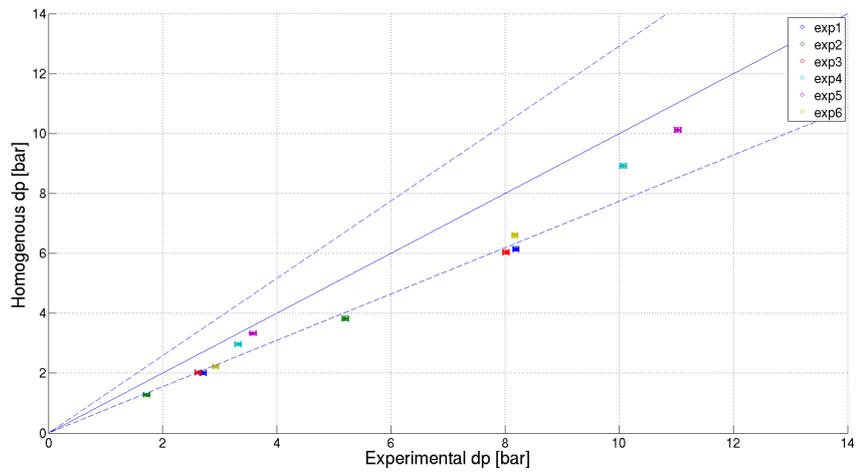$$\bar{e} = \Big(\frac{1}{N} \sum_i |z_i|\Big).\tag{8}$$

The mean error and the relative standard deviation have been computed, and the results are summarized in Table 3. Only the data points for the total pressure drop (between location 1 and 4) have been used in these calculations.

### 4.3. Discussion

As seen from Table 3, when considering all the present experiments, the Friedel model predicts the frictional pressure-drop the most accurately. The Cheng *et al.* model, on the other hand, predicts the frictional pressure-drop the least accurately. This may seem surprising, since the Cheng *et al.* model was developed specifically for $CO_2$ flows. The reason is probably that mass-flow rates in the experiments investigated in this work are much higher than what the Cheng *et al.* model was developed for. Thus, this is an indication that the significance of $CO_2$-specific insight (which is exploited in the Cheng *et al.* model) may be relatively small compared to the importance of a larger database of data (which is advantage of the Friedel model).

(a) Friedel model



(b) Cheng *et al.* model



(c) Homogeneous-flow model

Figure 3: Comparison between experimental and calculated frictional pressure drop.

Table 4: Friction-model error calculated based on the high flowing-vapor-fraction experiments.

| Model | $s_R$ (%) | $\bar{e}$ (%) |
|---|---|---|
| Friedel | 10.2 | 8.78 |
| Cheng *et al.* | 1.85 | 1.35 |
| Homogenous | 20.12 | 12.92 |

From Figure 3b, it seems like there is a large difference between how well the Cheng *et al.* model is able to predict the pressure drop for experiment number 4, 5, and 6 compared to 1, 2 and 3. One main difference between these two groups of experiments can be seen in Figure 2: Experiments 4, 5 and 6 are associated with a higher flowing vapor-fraction ($x = \dot{m}_g \gtrsim 0.6$). When only these "high flowing-vapor-fraction" experiments are considered, a substantial reduction in the computed standard deviation results for the Cheng *et al.* model, see Table 4. This may be a coincidence or an indication that the Cheng *et al.* model works better for higher vapor fractions. More experiments should be carried out to verify the indicated trend.

We will now compare the above results to those of Friedel [13] and Cheng *et al.* [9].

### 4.3.1. Comparison with Friedel's results

For all the horizontal single-component two-phase flow points in Friedel's database, Friedel calculated a relative standard deviation of 32 % [13, Tab. 3]. The fact that the relative standard deviation calculated in the present work (9.7 %) is lower, shows that the results obtained for the present experiments are better than expected. This may be an indication that the Friedel correlation is a suitable model for prediction pressure drop in $CO_2$ flows. However, it should be emphasized we cannot make a strong conclusion based on only six experiments.

### 4.3.2. Comparison with Cheng et al.'s results

The mass flow rates in the present experiments are much higher than what the Cheng *et al.* model [9] was developed for. Nevertheless, the model still estimated the frictional pressure-drop well for the high-flowing-vapor-fraction experiments.

Cheng *et al.* [9] compared 387 pressure-drop experiments for $CO_2$ to their own model and to the Friedel model, and found a mean error of 28.6 % and 30.9 %, respectively. This is higher than the results in the present work (19.93 % and 8.13 %), especially for the Friedel model. This may indicate that the Friedel model works better for $CO_2$ at higher mass flow rates than at lower mass flow rates.

## 5. Conclusions

Calculated frictional pressure drop using the Friedel model [13], the Cheng *et al.* model [9] and the homogenous model have been compared with six steady-state pressure-drop experiments [11].

- When all the six experiments are considered, the Friedel model is the most accurate with a standard deviation of 9.7 %. The Cheng *et al.* model is less accurate than the homogeneous model with a relative standard deviation of 57.74 % versus 29.18 %. This is an indication that the significance of $CO_2$-specific insight (which is exploited in the Cheng *et al.* model) is relatively small compared to the importance of a larger pressure-drop database (which is advantage of the Friedel model).

- The frictional pressure drop is underestimated for all experiments when using the homogenous model, and for the low-vapor-fraction experiments when the Cheng *et al.* model is used.

- When only the high-flowing-vapor-fraction (above 0.6) experiments are considered, the Cheng *et al.* model is the most accurate, with a relative standard deviation of only 1.85 %.

- The calculated relative standard deviation for the Friedel model was 9.7 % and thus much lower than the relative standard deviation for the large pressure-drop database used by Friedel [13] (32 %). This may be an indication that the Friedel model is just as suitable for predicting the pressure drop in $CO_2$ as for other fluids.

- The friction-model-input sensitivity and the sensor uncertainty are small compared to the uncertainty in the friction models themselves.

It should be noted that no strong conclusions can be made based only on the present six experiments. Therefore, it would have been interesting to include more experimental data in the analysis to see if the observed trends hold more generally. In particular, it would have been of interest to compare the Friedel model and the Cheng *et al.* model for conditions more similar to what would be the case in typical CCS applications. That means larger pipes and the presence of impurities. Further experiments could also be performed with pure $CO_2$ to confirm repeatability and to increase the spectrum of results.

### Acknowledgements

### References

[1] P. S. Ringrose, A. S. Mathieson, I. W. Wright, F. Selama, O. Hansen, R. Bissell, N. Saoula, J. Midgley, The In Salah $CO_2$ storage project: lessons learned and knowledge transfer, in: T. Dixon, K. Yamaji (Eds.), GHGT-11 – 11th International Conference on Greenhouse Gas Control Technologies, RITE / IEAGHG, Energy Procedia vol. 37, Kyoto, Japan, 2013, pp. 6226–6236. doi:10.1016/j.egypro.2013.06.551.

[2] Global CCS Institute, The global status of CCS, Tech. rep. (2012).

[3] IEA, Energy Technology Perspectives, 2012. doi:10.1787/20792603.

[4] S. T. Munkejord, C. Bernstone, S. Clausen, G. de Koeijer, M. J. Mølnvik, Combining thermodynamic and fluid flow modelling for $CO_2$ flow assurance, in: T. Dixon, K. Yamaji (Eds.), GHGT-11 – 11th International Conference on Greenhouse Gas Control Technologies, RITE / IEAGHGT, Energy Procedia, vol. 37, Kyoto, Japan, 2013, pp. 2904–2913. doi:10.1016/j.egypro.2013.06.176.

[5] P. Aursand, M. Hammer, S. T. Munkejord, Ø. Wilhelmsen, Pipeline transport of $CO_2$ mixtures: Models for transient simulation, Int. J. Greenh. Gas Con. 15 (2013) 174–185. doi:10.1016/j.ijggc.2013.02.012.

[6] A. Bredesen, A. Hafner, J. Pettersen, P. Nekså, K. Aflekt, Heat transfer and pressure drop for in-tube evaporation of $CO_2$, in: Proceedings of the International Conference on Heat Transfer Issues in Natural Refrigerants, IIF-IIR, University of Maryland, USA, 1997, pp. 1–15.

[7] J. Pettersen, Flow vaporization of $CO_2$ in microchannel tubes, in: 4th International Conference on Compact Heat Exchangers and Enhancement Technology for the Process Industries, Grenoble, France, 2002, pp. 111–121, Exp. Therm. Fluid Sci. 28 (2–3), 2004. doi:10.1016/S0894-1777(03)00029-3.

[8] R. Yun, Y. Kim, Two-phase pressure drop of $CO_2$ in mini tubes and microchannels, in: 1st International Conference on Microchannels and Minichannels, ASME, Rochester, NY, USA, 2003, pp. 259–270, Microscale Therm. Eng. 8 (3), 2004. doi:10.1080/10893950490477554.

[9] L. Cheng, G. Ribatski, J. M. Quibén, J. R. Thome, New prediction methods for $CO_2$ evaporation inside tubes: Part I – A two-phase flow pattern map and a flow pattern based phenomenological model for two-phase flow frictional pressure drops, Int. J. Heat Mass Tran. 51 (1–2) (2008) 111–124. doi:10.1016/j.ijheatmasstransfer.2007.04.002.

[10] F. Aakenes, Frictional pressure-drop models for steady-state and transient two-phase flow of carbon dioxide, Master's thesis, Department of Energy and Process Engineering, Norwegian University of Science and Technology (NTNU) (Jun. 2012).

[11] J. P. Jakobsen, G. Skaugen, A. Austegard, A. Hafner, M. Drescher, $CO_2$ pipeline test rig: Experiments and simulation – model verification, Tech. Rep. TR F6617, SINTEF Energy Research, Trondheim, Norway, restricted (Jan. 2008).

[12] G. de Koeijer, J. H. Borch, M. Drescher, H. Li, Ø. Wilhelmsen, J. Jakobsen, $CO_2$ transport - depressurization, heat transfer and impurities, in: J. Gale, C. Hendriks, W. Turkenberg (Eds.), GHGT-10 – 10th International Conference on Greenhouse Gas Control Technologies, IEAGHGT, Energy Procedia vol. 4, Amsterdam, The Netherlands, 2011, pp. 3008–3015. doi:10.1016/j.egypro.2011.02.211.

[13] L. Friedel, Improved friction pressure drop correlations for horizontal and vertical two phase pipe flow, in: Proceedings, European Two Phase Flow Group Meeting, Ispra, Italy, 1979, paper E2.

[14] G. de Koeijer, J. H. Borch, J. Jakobsen, M. Drescher, Experiments and modeling of two-phase transient flow during $CO_2$ pipeline depressurization, in: J. Gale, H. Herzog, J. Braitsch (Eds.), GHGT-9 – 9th International Conference on Greenhouse Gas Control Technologies, Energy Procedia vol. 1, Washington DC, USA, 2009, pp. 1649–1656. doi:10.1016/j.egypro.2009.01.220.

[15] J. G. Collier, J. R. Thome, Convective boiling and condensation, 3rd Edition, Oxford University Press, Oxford, UK, 1994.

[16] NIST, NIST Chemistry Webbook, http://webbook.nist.gov/chemistry/, accessed 2012-05-09 (2012).

## Appendix A.  The experimental data

In the present work, experimental data from the report of Jakobsen *et al.* [11] has been employed, see Tables A.5–A.7.

Table A.5: The measured temperature and pressure along the test section. See Figure 1.

| EXPNR | TT-30 | TT-40 | TT-50 | TT-60 | PIT-30 | PIT-40 | PIT-50 | PIT-60 |
|---|---|---|---|---|---|---|---|---|
| | (C) | (C) | (C) | (C) | (bar) | (bar) | (bar) | (bar) |
| 1 | 13.19 | 10.76 | 8.3 | 5.96 | 48.47 | 45.8 | 42.97 | 40.33 |
| 2 | 8.69 | 6.98 | 5.35 | 3.83 | 43.37 | 41.72 | 39.88 | 38.16 |
| 3 | 12.4 | 10.04 | 7.52 | 5.26 | 47.65 | 45.14 | 42.28 | 39.64 |
| 4 | 16.31 | 13.62 | 10.55 | 7.76 | 52.36 | 49.13 | 45.51 | 42.26 |
| 5 | 16.92 | 14.01 | 10.69 | 7.59 | 53.04 | 49.54 | 45.59 | 42.05 |
| 6 | 15.51 | 13.02 | 10.68 | 8.56 | 51.2 | 48.33 | 45.56 | 43.07 |

Table A.6: The temperature and pressure before the throttling valves, the mass flow rates and the surrounding temperature (TT-120 and TT-121).

| EXPNR | TT-20 | PT-20 | TT-122 | TT-123 | FE-10 | FE-20 | TT-120 | TT-121 |
|---|---|---|---|---|---|---|---|---|
| | (C) | (bar) | (C) | (C) | (kg/min) | (kg/min) | (C) | (C) |
| 1 | 3.37 | 66.82 | 28.53 | 2.9 | 1.9 | 5.93 | 11.52 | 11.35 |
| 2 | 10.02 | 60.38 | 27.02 | 9.51 | 1.22 | 3.76 | 11.45 | 11.28 |
| 3 | 2.49 | 60.51 | 22.78 | 1.83 | 2.86 | 3 | 8.98 | 10.5 |
| 4 | 0.27 | 56.93 | 20.07 | -0.19 | 4.68 | 1.61 | 11.11 | 12.4 |
| 5 | 9.98 | 54.78 | 18.55 | -0.13 | 4.96 | 1.73 | 13.16 | 15.21 |
| 6 | 6.66 | 55.77 | 22.35 | 6.21 | 3.85 | 1.27 | 13.18 | 14.85 |

Table A.7: The pressure drop between position 1 and 2, and 1 and 4. See Figure 1.

| EXPNR | PDT-41 | PDT-61 |
|---|---|---|
| | (bar) | (bar) |
| 1 | 2.71 | 8.2 |
| 2 | 1.72 | 5.2 |
| 3 | 2.63 | 8.02 |
| 4 | 3.32 | 10.07 |
| 5 | 3.58 | 11.03 |
| 6 | 2.93 | 8.17 |